AD-A268 800 MENTATION PAGE

	REPORT DATE	3. REPORT TYPE AND DATES COVERED	
	July 31, 1993	Annual	01 July 92-30 June 93

4. TITLE AND SUBTITLE
(U) Combustion Instability Phenomena of Importance to Liquid Propellant Engines

5. FUNDING NUMBERS
PE - 61102F
PR - 2308
SA - A1
G - AFOSR-91-0336

6. AUTHOR(S)

R. J. Santoro and W. E. Anderson

7. PERFORMING ORGANIZATION NAME(S) AND ADDRESS(ES)
The Pennsylvania State University
240 Research Building East, Bigler Road
University Park, PA 16802-2320

8. PERFORMING ORGANIZATION REPORT NUMBER

AEOSR-TR· 93 0667

9. SPONSORING MONITORING AGENCY NAME(S) AND ADDRESS(ES)
AFOSR/NA
110 Duncan Avenue, Suite B115
Bolling AFB, DC 20332-0001

DTIC
ELECTE
AUG 3 1 1993
S C D

10. SPONSORING MONITORING AGENCY REPORT NUMBER

11. SUPPLEMENTARY NOTES

12a. DISTRIBUTION AVAILABILITY STATEMENT

Approved for public release; distribution is unlimited.

12b. DISTRIBUTION CODE

93-20214

13. ABSTRACT Maximum 200 words.

A study examining impinging liquid jets has been underway to determine physical mechanisms responsible for combustion instabilities in liquid bi-propellant rocket engines. Primary atomization has been identified as an important process. Measurements of atomization length, wave structure, and drop size and velocity distribution were made under various ambient conditions. Test parameters included geometric effects and flow effects. It was observed that pre-impingement jet conditions, specifically whether they were laminar or turbulent, had the major effect on primary atomization. Comparison of the measurements with results from a two-dimensional linear aerodynamic stability model of a thinning, viscous sheet were made. Measured turbulent impinging jet characteristics were contrary to model predictions; the structure of waves generated near the point of jet impingement were dependent primarily on jet diameter and independent of jet velocity. It has been postulated that these impact waves are related to pressure and momentum fluctuations near the impingement region and control the eventual disintegration of the liquid sheet into ligaments. Examination of the temporal characteristics of primary atomization (ligament shedding frequency) strongly suggests that the periodic nature of primary atomization is a key process in combustion instability.

Impinging jet injectors, combustion instability, atomization

48

UNCLASSIFIED	UNCLASSIFIED	UNCLASSIFIED	UL

Annual Report
on
Combustion Instability Phenomena of Importance to
Liquid Propellant Engines

Prepared by:

Robert J. Santoro and William E. Anderson
Department of Mechanical Engineering
and
Propulsion Engineering Research Center
The Pennsylvania State University
University Park, PA 16802 - 2320

Submitted to:

Air Force Office of Scientific Research
Bolling Air Force Base
Washington, D.C.

July 1993

1.0 RESEARCH OBJECTIVE

Impinging jet injectors are a common type of injector used in liquid rocket engines and are typically used in engines where both propellants are injected as a liquid, e.g., engines using LOX/hydrocarbon and storable propellant combinations. Because they are much simpler to fabricate than coaxial injectors, they are also an attractive candidate for use in LOX/hydrogen engines. There is also a current interest in engines where both propellants are injected as gas; here, the impinging jet injector system would also be favored over coaxial jets due to its superior mixing characteristics.

The current state of impinging jet injector design analysis, however, significantly lags behind that for coaxial elements. A substantial problem exists with the current design analysis methodology for impinging jet injectors in that to increase the margin from unstable combustor operation, the combustor designer is faced with decrementing performance and thermal compatibility characteristics. Also, empirically-based analysis techniques are used which depend, of course, on existing engine data. Due to the empirical nature of stability analysis, and the very high costs of engine development, innovative designs that take advantage of current technology are not being used; instead, current engines are essentially being built with the same injector designs that were developed in the 1960's.
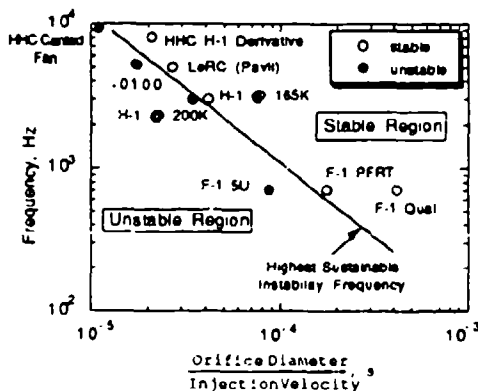

Fig 1. Hewitt stability correlation for determining the highest possible combustion instability frequency in rocket engines using impinging jet injectors as a function of injector stability parameter. Correlation effectiveness is illustrated by a few examples of LOX/hydrocarbon engines.

The present research program underway at the Propulsion Engineering Research Center at Penn State is focused on providing the requisite fundamental understanding for the development of an advanced, *a priori* combustion stability design analysis capability. This can only be achieved when the fundamental mechanisms of combustion stability in rocket engines using impinging jet injectors are understood. A key element of the program's approach is the use of a proven empirical stability correlation, previously a proprietary design tool at Aerojet shown in Fig. 1, that relates the highest possible frequency of combustion instability that can be driven by an injector with given geometric and operational parameters, i.e., injector diameter and injection velocity. A review and characteristic time analysis of potential combustion instability mechanisms that

explain the correlation has been performed,[1] resulting in the identification of the processes of primary and secondary atomization, inter-propellant mixing, and vaporization as likely important controlling steps. Identification of these processes has been used to define the dependent test variables to be measured: length of the intact liquid sheet, ligament shedding frequency, drop size and velocity distribution, and heat release rate. The empirical correlation is used to define independent test parameters: orifice diameter, injection velocity, and imposed frequency of oscillation.

The results of the review have also indicated that a clear understanding of primary atomization is of particular importance. Studies of primary atomization have shown that it occurs on a temporal scale that is similar in magnitude to combustion instability, and that the temporal dependency on orifice diameter and injection velocity is similar to the dependency indicated by the combustion stability correlation used in the present study. Furthermore, inter-propellant mixing and droplet vaporization are controlled by the distribution of drop size and velocity which is determined by primary atomization. Thus, the major effort to date has been in the characterization of the injector's geometric and flow effects on primary atomization under steady and atmospheric conditions. Measurements under forced acoustic and high pressure conditions commenced late in the current reporting period. Measurements under combusting conditions are planned for midway through the next reporting period.

In summary, the overall objective of this study is to determine the physical mechanisms that are responsible for the combustion stability characteristics of rocket engines that use impinging jet injectors. A proven empirical correlation is used to link the fundamental study underway to practical rocket combustors. Specific objectives include: extensive cold-flow experimental characterization of the primary atomization characteristics under steady and forced acoustic conditions; development of a mechanistic model of primary atomization that accurately accounts for the observed physics of atomization; combustion experiments using advanced optical diagnostic techniques to measure the overall combustion response of the impinging jet injector elements to an imposed oscillating flowfield; and use of a combustion response model, based on the results of the experimental and theoretical developments, to relate the fundamental studies to the empirical combustion stability correlation. Achievement of these objectives and fundamental understanding of the operative instability mechanisms will lead to *a priori* design analysis methodologies and implementation of engineering control strategies to enable design of stable, high-performing, and thermally compatible rocket combustors.

2

2.0 RESEARCH STATUS

The present study is concentrated on defining the operative mechanisms of combustion instability in rocket engines that use impinging jet injectors. General information regarding the combustion process in rocket engine combustors of all types is also an important byproduct of this research. A review conducted earlier[1] identified the combustion processes of primary atomization, secondary atomization, inter-propellant mixing, and droplet heating and vaporization as potential key mechanisms of combustion instability. The effort involves cold-flow studies of primary atomization, secondary atomization, and mixing under both steady and forced oscillatory conditions, as well as studies under combusting and oscillatory conditions to measure the combustion response of the impinging liquid jets in terms of the phase relationship between the oscillating pressure field and combustion. Most of the effort to date has centered around an extensive characterization of primary atomization under cold-flow and atmospheric pressure conditions, with recent work emphasizing high-pressure and forced oscillatory conditions. There has also been a parallel effort in developing an accurate model of primary atomization throughout the current reporting period. More detail of the work can be found in References 1, 2, and 3.
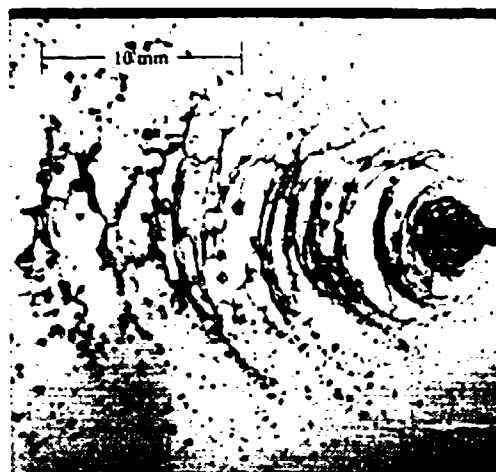
There are two clear reasons for emphasizing a detailed understanding of atomization in the study: (1) atomization provides the initial conditions for subsequent combustion processes by its determinant effect on drop size and velocity; and (2) the periodic nature of primary atomization (ligament shedding) has pronounced similarities to combustion oscillations in rocket engines in terms of both frequency range and the frequency dependency on injector operational and geometric parameters.

The three classical cases of fully-developed laminar jet flow, fully-developed turbulent jet flow, and "plug" jet flow have been studied. These cases were chosen because of their well-characterized velocity and turbulence intensity profiles. Absolute plug flow conditions were not obtained, but were approached by using orifices with short length-to-diameter ratios ($L/d_o \sim 5$). Short L/d_o orifices were operated either in the laminar or turbulent flow regime. Length-to-diameter ratios in impinging jet orifices used in rocket engines are typically about three. In addition to changing flow condition and L/d_o, other test parameters (see Table 1) included half-impingement angle, θ, orifice diameter, and free jet length prior to impingement.

It was obvious that the flow condition of the jet before impingement, i.e., whether it was laminar or turbulent, had the major effect on atomization. To illustrate the importance of the initial conditions of the liquid jet, consider the instantaneous images of the sheets formed by laminar and turbulent impinging jets shown in Fig. 2. These images were taken under quiescent conditions and at atmospheric pressure. Although the jet Reynolds numbers for both the laminar

3

<div style="text-align:center">(a)   (b)</div>

Fig. 2. Instantaneous images of sprays formed by two impinging water jets. (a) Resultant sheet formed by two laminar impinging jets emanating from 0.51 mm inner diameter, $L/d_0=375$ precision bore glass tubes. The jet velocity was 13.1 m/s and the full impingement angle, 2θ, was 60°. (b) Resultant sheet formed by two turbulent impinging jets emanating from 0.64 mm inner diameter, $L/d_0=80$ precision bore glass tubes. The jet velocity was 12.2 m/s and the full impingement angle, 2θ, was 60°.

and turbulent cases are similar, the resultant sheets have very different and distinct characteristics. In the laminar case, Fig. 2a, small ripples on the surface of the sheet are seen near the impingement point, and after some distance the sheet suddenly disintegrates into droplets. In many of the images of laminar impinging jets, incipient breakup occurred at mid-span of the sheet. Drops are also seen shedding off the edge of the sheet. In the turbulent case, Fig. 2b, the waves that appear at impact seem much larger than in the laminar case. Downstream, the sheet disintegrates into ligaments, with incipient breakup consistently occurring at the edges where the sheet is thinnest. Periodicity is indicated by waves on the liquid sheet and by the spacing between the detached ligaments. Examination of the detached liquid structures reveals irregular liquid shapes that contract into roughly cylindrical ligaments. The cylindrical ligaments appear to contract further into irregularly-shaped drops that will eventually take a nearly spherical shape. The ligament-to-droplet formation process is most likely controlled by surface tension-driven instabilities.

The turbulent sheet is not as symmetric as the laminar sheet, and, by comparing upstream and downstream points near the edge of the turbulent sheet there appears to be relatively large-scale displacement of the sheet in the image plane, indicating jet unsteadiness on the large scale. Examination of opposite edges at the same downstream location leads to the same conclusion

<div style="text-align:center">4</div>

regarding asymmetry and large-scale jet unsteadiness. This phenomena is in all probability three-dimensional.

From the results presented in Fig. 2, it is clear that the phenomena controlling atomization for impinging jet injectors is complicated and requires both theoretical and experimental study. Thus, during the current reporting period, emphasis has been given to comparing the non-vaporizing atmospheric impinging jet studies with theoretical models as well as extending the experimental work to higher ambient pressures and forced oscillatory conditions.

Table 1. Test Conditions

Test Parameter	Glass Tube Injector	Twist-Drilled Injector
Orifice Diameter, mm	0.64, 1.02, and 1.45	1.02
Impingement Angle, degrees	40, 60, 80, and 180	60
Length-to-Diameter Ratio	5, 35, 50, and 80	10
Pre-Impingement Length, mm	2.5, 25, and 35	14
Laminar Flow Conditions:	$2800 < Re_j < 10000$	N/A
	$200 < We_j < 2300$	N/A
Turbulent Flow Conditions:	$4000 < Re_j < 30000$	$3000 < Re_j < 20000$
	$300 < We_j < 7000$	$150 < We_j < 4000$
Ambient Pressure, atm	1	1, 6, and 9
Acoustic Frequency, Hz	N/A	668, 1362, and 2016
Acoustic Pressure, kPa (psi) (peak - peak amplitude)	N/A	1.4 - 6 (0.2 - 0.9)

2.1 Modeling Results

Two significant modeling tasks are undertaken under this contract. First, a mechanistic model of primary atomization that can accurately predict the effects of injector design and operation on breakup length, atomization frequency, and drop size and velocity distributions is critically needed by engine designers. This model also provides key input to the second modeling effort, a combustion response model. The combustion response model is needed to account for vaporization effects and to analyze the results from uni-element combustion tests for comparison to the empirical stability correlation. Efforts to date have been restricted to the atomization modeling.

The atomization model that has been used to date by most workers in this area[4,5,6] is based on a linear stability analysis of aerodynamically-induced wave growth on the surface of a thinning, viscous liquid sheet. This model can be used to predict breakup length, the periodic structure of breakup, and drop size. Details of our implementation of the model as well as a more detailed comparison with the present experimental results can be found in References 2 and 3 and Appendix 1.

In brief, the linear stability model is based on the growth of infinitesimal disturbances due to aerodynamic stresses on the liquid sheet surface to describe the disintegration of liquid sheets. The disturbance on the sheet surface, η, is given by

$$\frac{\eta}{\eta_o} = e^{\beta_i t} \tag{1}$$

where η_o is the initial displacement amplitude, β_i is the growth rate and t is time.

Typically the growth rate, β_i, is calculated for a spectrum of wavenumbers, k. The disturbance wavenumber corresponding to the maximum growth rate, $\beta_{i,m}$, controls the breakup process. Both sinuous (antisymmetric) and dilatational (symmetric) waves can grow; however, previous research indicates that sinuous waves grow faster than dilatational waves,[6] hence only the behavior of sinuous disturbances were considered. The theory does not predict a critical disturbance amplitude for sheet disintegration, and consequently, an empirical relation of the following form is typically used:[2]

$$\int_0^{t_b} \beta_{i,m} dt = \int_0^{x_b} \frac{\beta_{i,m}}{U_s} dx = 12 \tag{2}$$

where t_b is the sheet breakup time, x_b is the breakup length, and U_s is the sheet velocity. The fastest growing wave and its growth rate are found from the general dispersion equation:

$$\beta^2_{i,nd} + \frac{(kh)^2}{Re_s}\beta_{i,nd} + 2s(kh)^2\left(\frac{1}{sWe_s} - \frac{1}{kh}\right) = 0 \qquad (3)$$

where;

$$\beta_{i,nd} = \frac{\beta_i h}{U_s}, \qquad\qquad Re_s = \frac{\rho_l U_s h}{\mu_l}, \qquad\qquad We_s = \frac{\rho_l U_s^2 h}{\sigma}.$$

where h is the sheet thickness and s is the ratio of the gas density to the liquid density. The first term in Equation (3) is associated with momentum in the displacement direction, the second term rises from viscous forces while the two parts of the third term account for surface tension forces and aerodynamic forces, respectively. Drop size can also be calculated by assuming the sinuous waves that are formed on the sheet break at their crests and troughs and subsequently contract into cylindrical ligaments with diameter d_L. Drops are formed when the cylindrical ligaments undergo the well-known process of capillary instability and pull themselves into spheres (drops) with a diameter, d_D, which, under the conditions of the present study, can be expressed by
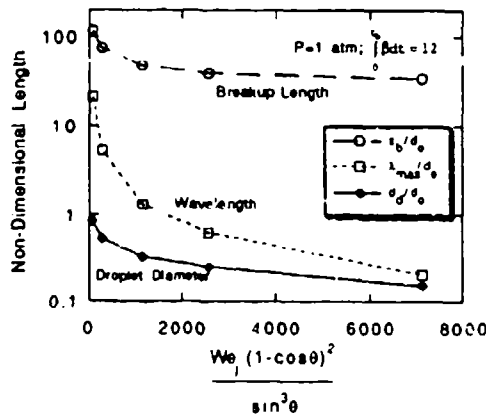
$$d_D \approx 1.89 d_L \qquad (4)$$

Fig. 3. Non-dimensional lengths as a function of geometrically scaled jet Weber number as predicted by aerodynamic instability model. Lengths normalized by orifice diameter.

In the course of analyzing results from the aerodynamic stability model, a non-dimensional scaling parameter based on the jet Weber number, $We_j = \rho_j v_j^2 d_o/\sigma$, and the half-impingement angle, θ, was identified: $We_j(1-\cos\theta)^2/\sin^3\theta$. Use of this parameter collapses the theoretical dependence of breakup length, fastest-growing wavelength, and drop size on orifice diameter, impingement angle, and velocity into a single curve dependent on the scaling parameter. Results from the model are shown in Fig. 3, where non-dimensional lengths, normalized by the orifice diameter, d_o, are plotted against the geometrically scaled jet Weber number.

7

2.2   Experimental Results

During the current reporting period, experiments were performed at atmospheric conditions using impinging jet injectors made of either precision bore glass tubes or twist-drilled orifices in a brass block. The latter injector unit was also used in experiments at high pressure and under oscillatory conditions forced by an acoustic driver. Table 1 summarizes the test parameters to date.

2.2.1   Atmospheric Pressure Atomization Studies

Length measurements of the intact sheet and of periodic structures were made from images such as those shown in Fig. 2. Non-dimensional breakup length, x_b/d_o, is plotted against jet Weber number in Fig. 4 for laminar and turbulent impinging jet cases. Clear differences between the two cases can be seen. The non-dimensional breakup length of the turbulent impinging jets appears to have some dependence on impingement angle, but appears to be relatively independent of jet Weber number. There is a strong dependence on jet Weber number for the laminar impinging jet case.
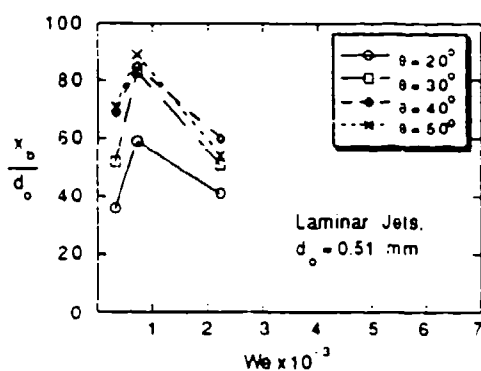

Fig. 4a. Non-dimensional breakup length of laminar impinging jets from precision bore glass tubes as a function of jet Weber number.
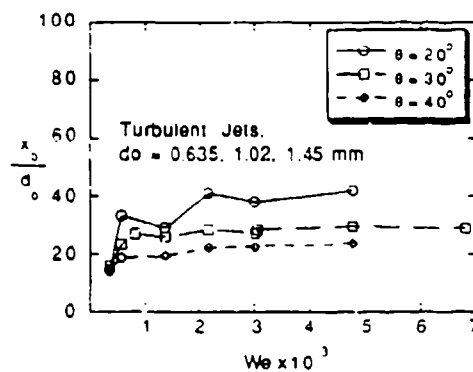
Fig. 4b. Non-dimensional breakup length of turbulent impinging jets from precision bore glass tubes as a function of jet Weber number.

Comparisons of the measured non-dimensional breakup length with predictions from the aerodynamic instability model are shown in Fig. 5. Again the differences between the turbulent impinging jet case and the laminar impinging jet case are evident. Laminar impinging jet breakup may be modeled relatively well by the aerodynamic instability model, but again, the turbulent impinging jet breakup shows little dependence on the geometrically scaled jet Weber number. It appears that turbulent impinging jet breakup, which is clearly dependent on orifice diameter and impingement angle, is related to the sheet thickness, which also is determined by orifice diameter and impingement angle .
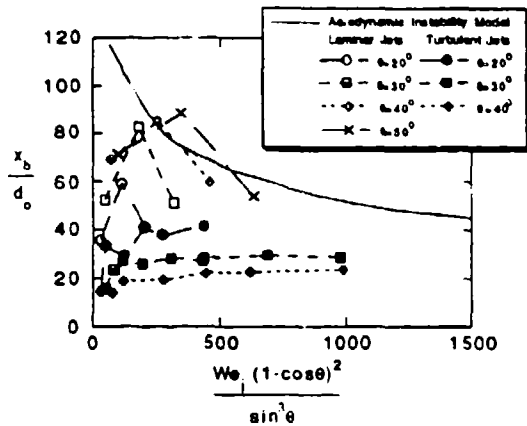
Fig 5. Non-dimensional breakup length as a function of geometrically scaled jet Weber number. Comparison of measurements with aerodynamic instability model predictions.
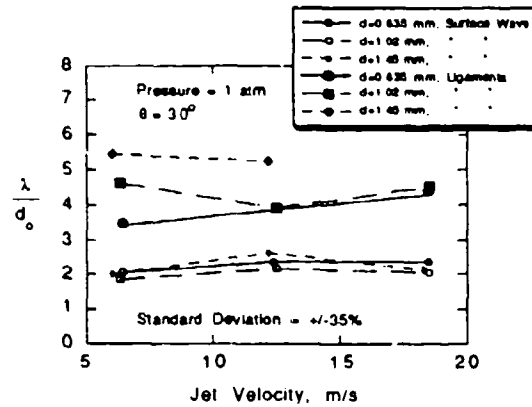
Fig. 6. Non-dimensional distance measured between adjacent surface wave structures and between adjacent ligaments.

The measured distance normalized by orifice diameter of the separation between periodic structures for turbulent impinging jets is shown in Fig. 6 as a function of jet velocity. The "wavelength" appears to be primarily dependent on orifice diameter and independent of jet velocity. The observation of independence from jet velocity is contrary to the aerodynamic instability model predictions. The distance between detached ligaments is approximately constant at around 4 orifice diameters, and the distance between surface wave structures is constant at around 2 orifice diameters. There was a rather large spread in the data, with a standard deviation of +/- 35%.
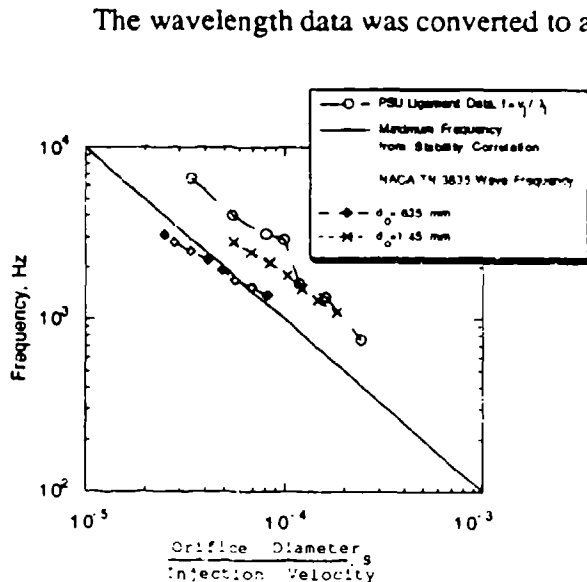
The wavelength data was converted to atomization frequency simply by dividing the jet velocity by the measured wavelength. Earlier studies[2] showed that measured drop velocities were nearly equal to the jet velocity. Atomization frequency data is presented in Fig. 7 based on ligament spacing. Also shown is "wave frequency" data from experiments of Heidmann et al.[7] These atomization frequencies are quite similar to the maximum possible combustion instability frequency given by the Hewitt Stability Correlation, also shown in Fig. 7. The similar dependencies of maximum possible instability frequency and atomization frequency on d_o/v_j is significant in terms of primary

Fig. 7. Comparison of measured atomization frequency with maximum combustion instability frequency from Hewitt Stability Correlation.
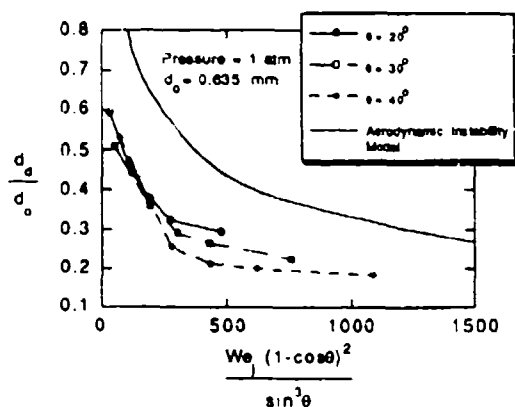
9

Fig. 8. Non-dimensional drop diameter as a function of geometrically scaled jet Weber number. Comparison of PDPA Measurements with predictions from aerodynamic instability model.

atomization being a key process in combustion instability.

Of course, the combustion process must also be considered in an analysis of combustion instability. In liquid rocket engine combustion, vaporization is the rate-limiting step. The vaporization process is controlled in large by the drop size. Accurate measurements of the drop size distribution are necessary to develop an accurate understand'- ' of the problem of combustion instability. An argon-ion based, two-component Phase Doppler Particle Analyzer (PDPA) was used for making drop size and velocity measurements. A description of the theoretical and operating principles of the PDPA are given elsewhere.[3] Non-dimensional arithmetic mean drop diameters (D_{10}) are presented in Fig. 8 for the turbulent impinging jet case. A comparison of measured D_{10} with the monodisperse drop size predicted by the aerodynamic instability model is also shown. The model predictions match the experimental trend quite well, and that the measurements appear to collapse into a single curve when plotted against the geometrically scaled jet Weber number as the model predicts. An empirical correlation for normalized drop size as a function of the geometrically scaled jet Weber number, $We_j f(\theta)$, was obtained with a correlation coefficient of 0.964:

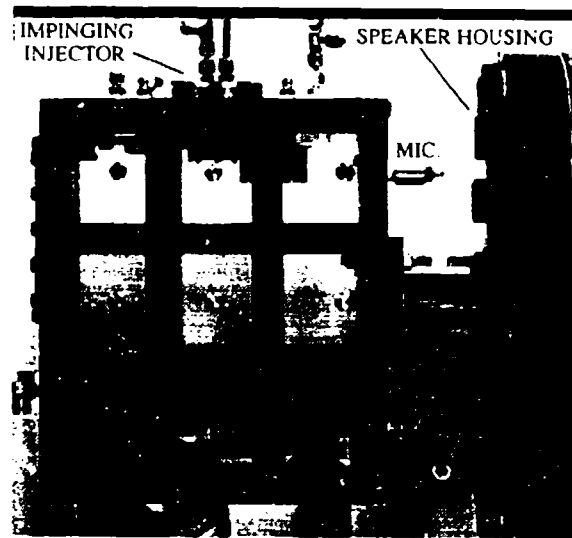$$\frac{d_D}{d_o} = 2.217 \cdot \{We_j f(\theta)\}^{-0.354} \tag{5}$$

2.2.2   High Pressure Atomization Studies

Recent experimental work in the current reporting period has focused on spray measurements using a transparent acoustic chamber emphasizing effects of applied acoustic fields and increased ambient pressure on spray formation processes. As with the quiescent, atmospheric pressure case, measurements made within the confines of the acoustic chamber include sheet breakup length and drop size distribution which will subsequently be discussed after a brief overview of the acoustic chamber and impinging injector characteristics.

An image of the transparent acoustic chamber is shown in Fig. 9. The interior dimensions of the chamber are 254 mm in width, 305 mm in height and 102 mm in depth. Two large Plexiglas faces allow visual access into the chamber, while steel grids brace the Plexiglas for

pressurized studies. The maximum chamber pressure is approximately 1.03 MPa (150 psia). A number of ports have been drilled into the chamber walls to allow for acoustic field measurements using microphones. An Altec Lansing compression driver, model 290-8k, is attached to the chamber right side-wall and is encased in a 241 mm (9.5 in.) inner diameter steel pressure vessel. The speaker is enclosed in the pressure vessel to keep equal pressure across the acoustic driver diaphragm during pressurized experiments. The Altec Lansing speaker is driven at a particular frequency using a Stanford Instruments function generator, model DS 345, and a Carver amplifier, model M-0.5t, having a gain of 30 dB. A PCB microphone, model 106B, and a PCB power supply, model 480D06, were used together to measure the oscillatory pressure field within the chamber. The sensitivity of the PCB microphone is approximately 0.04 mV/Pa (300 mV/psi).

Fig. 9. An image of the transparent acoustic chamber. The interior dimensions of the chamber are 254 mm in width, 305 mm in height, and 102 mm in depth. An acoustic compression driver is encased in a steel cylindrical pressure vessel attached to the right side-wall of the chamber. The impinging jet injector is inserted into the top plate of the chamber.
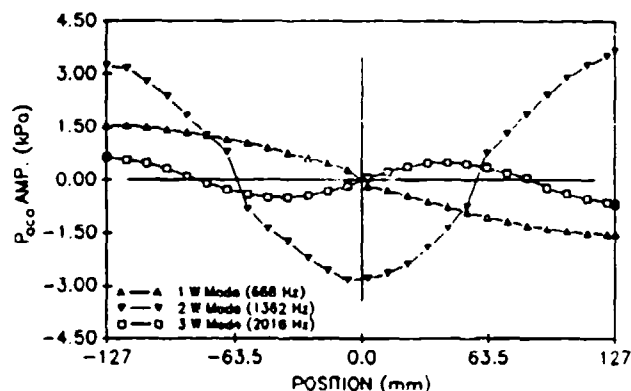
The twist-drilled impinging element fits into the top plate of the chamber. Water flows through a 41.3 mm inner diameter stilling chamber fitted with a sintered brass disc before entering the two 1.01 mm diameter injector orifices. Other twist-drilled impinging injector design information is given in Table 1.

The acoustic chamber was designed to excite the first (1W), second (2W) and third (3W) resonant modes in the 254 mm width dimension at frequencies on the order of several thousand hertz under ambient temperature conditions for air and helium environments. These modes and frequencies were chosen because of their similarity to typical rocket instabilities. This frequency range also allows for tests in stable and unstable regions according to the Hewitt stability correlation for realistic injector stability parameter values. Also, an acoustic driver was chosen with its highest efficiency in the thousand hertz range.

To ensure that the resonant mode of interest was achieved, pressure measurements were made with the PCB microphone attached to a long, thin stainless steel tube, which allowed for easy probing of the chamber interior. Extensive acoustic measurements were taken at the three resonant modes to characterize the dimensionality of the applied acoustic field. In short, the excited 1W, 2W and 3W modes, which had frequencies of 668 Hz, 1362 Hz and 2016 Hz, respectively, were primarily one-dimensional with minor variations in wave amplitude from the top to bottom of the chamber. Fig. 10 shows the measured pressure amplitude as a function of position across the chamber width at atmospheric pressure. The measurements were taken from a port at the speaker side-wall (position=127 mm) near the bottom of the chamber. Note that the shape of the wave- forms are very similar to the expected first through third standing wave modes. All three wave- forms were generated with the same input voltage and amplifier gain to the speaker. The peak pressure amplitude for the 2W mode is approximately 3.0 kPa (0.44 psi) at the center of the chamber, and is greater than the other two modes. The maximum observed pressure amplitude is approximately 1.5 kPa (0.22 psi) for the 1W mode and 0.70 kPa (0.10 psi) for the 3W mode.

Fig. 10. The measured acoustic pressure amplitude plotted as a function of position along the chamber width for the 1W, 2W, and 3W resonant modes at a chamber pressure of one atmosphere.
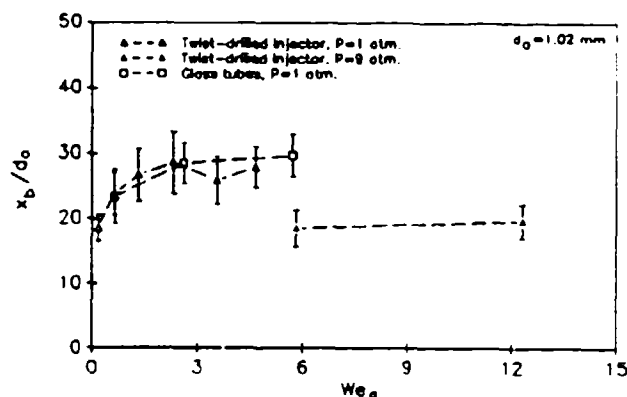

The effects on spray formation of oscillating velocity and of oscillating pressure can both be evaluated at the chamber centerline where the injector is oriented by exciting the 1W and 2W mode, respectively. Since the intended resonant acoustic mode structures are satisfactory, the effects of the applied acoustic field on the impinging jet spray and their relation to the Hewitt stability correlation can be pursued.

Again, measurements of breakup length, x_b, and drop size were made at high pressure and under oscillatory conditions. The spray breakup length, x_b, was measured at chamber pressures of one and nine atmospheres. The measurements were made from instantaneous spray images taken using a CID solid state camera in conjunction with a strobe light. A plot of the non-dimensional breakup length, x_b/d_o, as a function of We_j $(=\rho_j v_j^2 d_o/\sigma)$ is shown in Fig. 11. Each symbol in Fig. 11 represents an average of 17 individual breakup length measurements, while the

bars represent the plus/minus standard deviation of those measurements. Notice that the non-dimensional breakup length observed for the twist-drilled injector is quite similar to that of the glass tubes at a chamber pressure of one atmosphere. In both cases, the breakup length gradually increases with increasing gas Weber number.

Fig. 11. Non-dimensional breakup length as a function of the gas Weber number and injector type. Breakup length measurements for the twist-drilled injector were taken at pressures of one and nine atmospheres.

One of the major differences between the glass tubes and the twist-drilled injector is the orifice length-to-diameter ratio, L/d_o. The glass tube L/d_o is 80 while that of the twist-drilled injector is about ten. This observation that the length-to-diameter ratio does not appreciably affect the impinging jet spray breakup length was noted by Anderson et al.[2] In addition, the length of the free jet prior to impingement was 25.4 mm for the glass tube case and approximately 14.3 mm for the twist-drilled injector. Anderson et al.[2] also discussed the importance of this parameter on spray formation processes. At a chamber pressure of nine atmospheres, the non-dimensional breakup length decreases slightly when compared to the measurements made at one atmosphere.
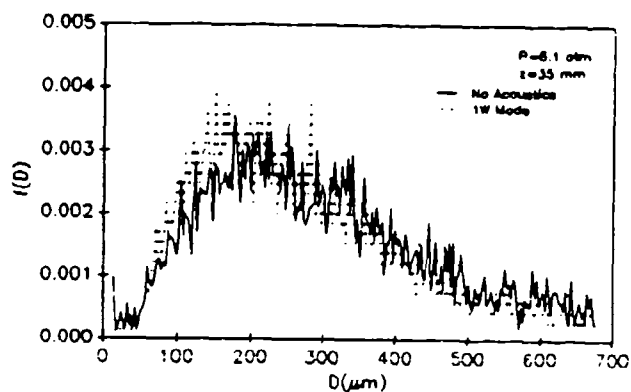
Curtains of air across portions of the chamber's Plexiglas walls were used to keep water wetting to a minimum. Breakup length measurements could not be obtained at higher Weber numbers and at higher chamber pressures because of an inability to acquire high contrast images due to the nature of the turbulent spray as well as lighting problems caused by excessive window wetting. Improvements in window cleaning and lighting practices are needed to make measurements at higher Weber numbers at pressurized conditions.

Drop size measurements were made using the PDPA along the spray centerline which coincides with the chamber centerline at a distance of 35 mm downstream of the impingement point. Axial and transverse (across the chamber width) drop velocities were measured. The injection velocity of the water through the twist-drilled injector was 9.0 m/s. Six thousand individual drop size and velocity measurements were made. Appreciable differences in the arithmetic mean diameter, D_{10}, at chamber pressures of one and six atmospheres were not found; however, the mean axial drop velocity decreased from 7.9 m/s to 6.8 m/s with the increased

pressure. From the limited data set, higher air densities within the chamber seem to have more of an effect on the drop speed and sheet length than drop size.

Next, the effects of an applied acoustic field were investigated by subjecting the impinging jet spray to the 1W mode at 668 Hz. Hence, a pressure node (oscillating velocity) existed at the chamber centerline where the measurements were made. The applied 1W acoustic field did not have an appreciable effect on drop size or drop velocity at the prescribed measurement location for a chamber pressure of one atmosphere. The acoustic field did, however, noticeably affect the drop formation process at a higher chamber pressure of six atmospheres, i.e., the applied 1W mode acoustic field seemed to enhance the atomization of the liquid sheet at the higher chamber pressure. Similar observations have previously been made in our laboratory[8] with jets, where it was observed that acoustic effects appeared only at higher ambient pressure. A smaller arithmetic mean drop size, approximately 236 μm, was measured for the acoustically perturbed case than the non-acoustic case, $D_{10} = 250$ μm. A plot of the drop size number distribution, f(D), versus measured drop diameter, D, for acoustically and non-acoustically perturbed cases is illustrated in Fig. 12. Evident from Fig. 12 is the higher drop number distribution between diameters of 100 to 200 μm for the acoustically perturbed case. This contributes to the observed lower arithmetic mean diameter.

Fig. 12. Drop size number distribution, f(D), measured by the PDPA at 35 mm downstream of the impingement point. Solid and dotted lines represent the number distribution without and with an applied acoustic field (1W mode), respectively. Ambient pressure is 6 atmospheres.

Both the breakup length and drop size/velocity results indicate that ambient pressure and oscillatory conditions affect the spray formation process markedly. Ongoing work is focused on obtaining further drop size measurements at various locations within the acoustic chamber.

2.3 Summary

In summary, a systematic study of the atomization of impinging liquid jets investigating the effects of jet conditions, orifice diameter, impingement angle, and jet velocity at quiescent, atmospheric conditions has been conducted. Preliminary studies of the effects of high pressure and forced oscillatory conditions were also conducted and are being continued. Results of these experimental studies have been compared to current theories in terms of sheet breakup length, wave structure, and drop size. Experiments contrasting laminar and turbulent jet conditions clearly demonstrate that the jet conditions have a dramatic effect on the atomization process. Specifically, the measured breakup lengths for laminar impinging jets are longer and displayed different trends as a function of jet velocity and impingement angle than those for turbulent impinging jets. In addition, the measured spray width for the turbulent impinging jet case remained approximately constant as a function of jet velocity and impingement angle for a fixed orifice diameter, unlike the laminar impinging jet case. The present results are in agreement with earlier studies at atmospheric pressure by Dombrowski and Hooper,[9] who speculated that these differences were due to velocity profile differences between fully-developed laminar flow and fully-developed turbulent flow. Based on the observations in our laboratory, however, it appears more likely that large pressure and momentum fluctuations near the impingement point determine the breakup characteristics of turbulent impinging jets, and are responsible for the obvious differences between laminar and turbulent cases. A quantitative assessment of the specific mechanisms controlling atomization remains to be established.

Comparisons of the experimental results at atmospheric pressure were also made with results from a linear stability-based theory. The model predicted a monotonically decreasing sheet breakup length with increasing Weber number which is opposite to the trend observed for turbulent impinging jets. Thus, the use of the aerodynamic instability model for describing sheet breakup appears to be incorrect, at least for the conditions of these studies.

Measurement of surface wave and periodic ligament formation phenomena for turbulent impinging jets indicates that the observed wavelengths are directly proportional to the orifice diameter and independent of jet velocity and impingement angle, which is also contrary to results from the model that predicts a strong dependence of these variables on jet velocity. It is interesting, however, that the aerodynamic instability model does provide quite a reasonable predictive capability for drop size. Recent measurements made in a high-pressure acoustic chamber indicate that there may be some effects of ambient pressure at greater than atmospheric pressure, and that is one of the current subjects of experimentation in our laboratory.

Based on the results of the above studies, approaches to modeling impinging jet atomization should focus on pre-impingement jet conditions and the physics near the jet impingement point, specifically the source of the observed impact waves that appear to control

turbulent impinging jet breakup. No current models address these phenomena. Additionally, the relationship between the periodic wave and ligament structures observed in these studies needs to be considered in light of their potential to initiate and sustain combustion instability phenomena associated with impinging jet rocket engine injectors.

3.0 FUTURE WORK

Efforts over the next reporting period will focus on completion of the high-pressure, acoustic cold-flow atomization and spray characterization studies. Measured variables will be breakup length, atomization frequency, and drop size and velocity distribution. The short L/d_o, twist-drilled injector element will be used in this study. Concurrent with the ongoing cold flow studies is the design and fabrication of a chamber for combustion tests. Again, like the cold flow studies, the impetus behind the chamber design is to gain insight into the fundamental processes that contribute to the ability of the Hewitt correlation to predict combustion instability. The primary atomization model development effort will also continue.

Combustion response modeling is a straightforward and extensively used method to analyze combustion instability. A simple combustion response model is also planned here, however with one major improvement over previous efforts: real atomization effects in terms of the periodicity of primary atomization and the polydisperse nature of the droplet field will be considered. If an appropriate mechanistic atomization model is not available for use with the combustion response model, an empirical model of atomization based on cold-flow studies will be developed and used.

Combustion measurements at realistic chamber and injector conditions are critical to defining combustion instability mechanisms. A conceptual design of an optically-accessible combustion chamber has been developed. The first chamber will be designed for 100 psi chamber pressure. Currently, it is planned to use a rotating gear with teeth to drive pressure oscillations. The rotating gear will be placed at the chamber's side-wall to drive waves transverse to the impinging jet's mean direction of flow. Injector elements will be placed strategically to allow the discrimination of oscillatory pressure effects from oscillatory velocity effects. Ethanol will be used as the liquid fuel. Measurements will be phase-locked to the pressure oscillations, and will include combustion light measurements (OH or CH radical emission) and drop size and velocity measurements. The combustion response model will be used to analyze the combustion test results. Unsteady atomization and drop distribution effects will be accounted for in the analysis.

4.0 REFERENCES

[1] Anderson, W. E., Ryan, H. M., and Santoro, R. J., "Combustion Instability of Importance to Liquid Bi-Propellant Rocket Engines." 28th JANNAF Combustion Meeting, San Antonio, TX, Oct. 28 - Nov. 1, 1991.

[2] Anderson, W. E., Ryan, H. M., Pal, S., and Santoro, R. J., "Fundamental Studies of Impinging Liquid Jets," AIAA paper 92-0458, 30th Aerospace Sciences Meeting, Reno, NV, Jan. 6 - 9, 1992.

[3] Ryan, H. M., Anderson, W. E., Pal, S., and Santoro, R. J., "Atomization Characteristics of Impinging Liquid Jets," AIAA paper 93-0230, 31st Aerospace Sciences Meeting, Reno, NV, Jan. 11 - 14, 1993 (accepted for publication in Journal of Propulsion and Power).

[4] Couto, H. S. and Bastos-Netto, D., "Modeling Drop Size Distribution from Impinging Jets," J. Propulsion, July-August 1991, pp. 654-656.

[5] Dombrowski, N. and Johns, W. R., "The Aerodynamic Instability and Disintegration of Viscous Liquid Sheets," Chem. Eng. Science, Vol. 18, 1963, pp. 203-214.

[6] Brodkey, R. S., Phenomena of Fluid Motions, Addison-Wesley Series in Chemical Engineering, 1967.

[7] Heidmann, M. F., Priem, R. J. and Humphrey, J. C., "A Study of Sprays Formed by Two Impinging Jets," NACA Technical Note 3835, March 1957.

[8] Hoover, D.V., Ryan, H.M., Pal, S., Merkle, C.L., Jacobs, H.R., and Santoro, R.J., "Pressure Oscillation Effects on Jet Breakup," Heat and Mass Transfer in Spray Systems, C. Presser and A.K. Gupta (eds.), HTD-Vol. 187, The American Society of Mechanical Engineers, New York, 1991, pp. 27 - 36.

[9] Dombrowski, N. and Hooper, P. C., "A Study of the Sprays Formed by Impinging Jets in Laminar and Turbulent Flow," J. Fluid Mechanics, Vol. 18, Part 3, 1963, pp. 392-400.

5.0 PUBLICATIONS

1. Anderson, W. E., and Santoro, R. J., "Primary Atomization Mechanisms of Impinging Jet Injectors," First Annual Symposium on Liquid Rocket Engine Combustion Instability, University Park, PA, Jan. 18 - 20, 1993 (accepted for publication in AIAA Progress Series on Liquid Rocket Engine Combustion Instability).

2. Ryan, H.M., Anderson, W.E., Pal, S., and Santoro, R.J., "Atomization Characteristics of Impinging Liquid Jets," AIAA paper 93-0230, 31st Aerospace Sciences Meeting, Reno, NV, Jan. 11 - 14, 1993 (accepted for publication in Journal of Propulsion and Power).

3. Ryan, H.M., Anderson, W.E., Pal, S., and Santoro, R.J., "Combustion Instability Phenomena of Importance to Liquid Propellant Engines," Propulsion Engineering Research Center Fourth Annual Symposium, Marshall Space Flight Center, Huntsville, AL, Sept. 9 - 10, 1992.

4. Anderson, W.E., Ryan, H.M., Pal, S., and Santoro, R.J., "Fundamental Studies of Impinging Liquid Jets," AIAA paper 92-0458, 30th Aerospace Sciences Meeting, Reno, NV, Jan. 6 - 9, 1992.

5. Hoover, D.V., Ryan, H.M., Pal, S., Merkle, C.L., Jacobs, H.R., and Santoro, R.J., "Pressure Oscillation Effects on Jet Breakup," Heat and Mass Transfer in Spray Systems, C. Presser and A.K. Gupta (eds.), HTD-Vol. 187, The American Society of Mechanical Engineers, New York, 1991, pp. 27 - 36.

6. Anderson, W.E., Ryan, H.M., and Santoro, R.J., "Combustion Instability of Importance to Liquid Bi-Propellant Rocket Engines," 28th JANNAF Combustion Meeting, San Antonio, TX, Oct. 28 - Nov. 1, 1991.

7. Santoro, R.J., "A Summary of The JANNAF Workshop on Diagnostics", 28th JANNAF Combustion Subcommittee Meeting, San Antonio, TX, Oct. 28 - Nov. 1, 1991.

6.0 PARTICIPATING PROFESSIONALS

Professor Robert J. Santoro, Professor of Mechanical Engineering

Mr. William E. Anderson, Graduate Student, Department of Mechanical Engineering

Mr. Harry M. Ryan, Graduate Student, Department of Mechanical Engineering

Mr. Shamim Rahman, Graduate Student, Department of Mechanical Engineering

Dr. Sibtosh Pal, Research Associate, Department of Mechanical Engineering

Mr. Ecton English, Visiting Undergraduate Student, Department of Mechanical
   Engineering, University of Maryland

Mr. Larry Schaaf, Engineering Assistant, Department of Mechanical Engineering

7.0 MEETINGS AND PRESENTATIONS

1. Anderson, W. E., and Santoro, R. J., "Primary Atomization Mechanisms of Impinging Jet Injectors," First Annual Symposium on Liquid Rocket Engine Combustion Instability, University Park, PA, Jan. 18 - 20, 1993.

2. Ryan, H.M., Anderson, W.E., Pal, S., and Santoro, R.J., "Atomization Characteristics of Impinging Liquid Jets," 31st Aerospace Sciences Meeting, Reno, NV, Jan. 11 - 14, 1993

3. Ryan, H.M., Anderson, W.E., Pal, S., and Santoro, R.J., "Combustion Instability Phenomena of Importance to Liquid Propellant Engines," Propulsion Engineering Research Center Fourth Annual Symposium, Marshall Space Flight Center, Huntsville, AL, Sept. 9 - 10, 1992.

4. Anderson, W.E., Ryan, H.M., Pal, S., and Santoro, R.J., "Fundamental Studies of Impinging Liquid Jets," 30th Aerospace Sciences Meeting, Reno, NV, Jan. 6 - 9, 1992.

5. Hoover, D.V., Ryan, H.M., Pal, S., Merkle, C.L., Jacobs, H.R., and Santoro, R.J., "Pressure Oscillation Effects on Jet Breakup," 1991 ASME Winter Annual Meeting, Atlanta, GA, Dec. 1 - 6, 1991.

6. Anderson, W.E., Ryan, H.M., and Santoro, R.J., "Combustion Instability of Importance to Liquid Bi-Propellant Rocket Engines," 28th JANNAF Combustion Meeting, San Antonio, TX, Oct. 28 - Nov. 1, 1991.

7. Santoro, R.J., "A Summary of The JANNAF Workshop on Diagnostics", 28th JANNAF Combustion Subcommittee Meeting, San Antonio, TX, Oct. 28 - Nov. 1, 1991.

8.0 INTERACTIONS

Throughout this research effort, extensive interactions with a number of personnel from Aerojet Propulsion Division of Sacramento, CA, have occurred. These interactions have involved Drs. Richard LaBotz and Darby Makel, and Messrs. Jerry Pieper, James Hulka, and Ross Hewitt. Specific interactions with Aerojet have been:

(1)   Aerojet has provided uni-element impinging jet injectors representative of the XLR-132, Transtage, and F-1 engines for study.

(2)   R.J. Santoro, S. Pal, and S. Rahman visited Aerojet in December, 1992 to present results from this and associated studies.

(3)   R. LaBotz, D. Makel, and R. Hewitt have visited Penn State on separate occasions to review research results and plans, the latest occurring on July 23 and 24, 1992 by R. Hewitt to discuss acoustic chamber and study injector element designs.

Near-term plans for further interactions with Aerojet include a trip by J. Pieper to Penn State in October, 1993 to review research results and combustion experiment plans.

Additional interactions have occurred with Rocketdyne engineers, who are also very interested in the results of our study. Specifically, Mr. Steven Fisher and Dr. Robert Jensen have visited our laboratory to discuss research results and future plans.

APPENDIX 1

Atomization Characteristics of Impinging Liquid Jets

AIAA paper 93-0230

Presented at the 31st Aerospace Sciences Meeting
Reno, NV
Jan. 11 - 14, 1993

accepted for publication in <u>Journal of Propulsion and Power</u>, July, 1993

AIAA 93-0230

Atomization Characteristics of Impinging Liquid Jets

H. M. Ryan, W. E. Anderson,
S. Pal and R. J. Santoro

The Pennsylvania State University
University Park, PA

31st Aerospace Sciences Meeting & Exhibit
January 11-14, 1993 / Reno, NV

ATOMIZATION CHARACTERISTICS OF IMPINGING LIQUID JETS

H.M. Ryan[*], W.E. Anderson[*], S. Pal[**] and R.J. Santoro[†]
Propulsion Engineering Research Center
and
Department of Mechanical Engineering
The Pennsylvania State University
University Park, PA 16802

Abstract

The atomization characteristics of sheets formed by both laminar and turbulent impinging jets were experimentally studied as a function of flow and injector geometric parameters. In particular, sheet breakup length along the sheet centerline, maximum sheet width, distance between adjacent waves apparent on the sheet and drop size distributions were measured. A linear stability-based model was used to determine the most unstable wavenumber and the corresponding growth rate factor on two-dimensional diminishing inviscid and viscous sheets. These wave characteristics were used to predict both the sheet breakup length and the resulting drop sizes. The predictions were then compared to the experimental results. A second model, applicable for low Weber number regions, in which sheet disintegration is caused by stationary antisymmetric waves, was used to predict the shape of the sheet formed by two impinging liquid jets. Again, comparisons with experimental measurements were made.

The linear stability-based theory predictions of breakup length as a function of jet velocity did not agree in trend or magnitude with experimental measurements. However, for Weber numbers less than 350, the measured breakup length and width for laminar impinging jets were well predicted by the stationary antisymmetric wave-based model. Finally, drop size predictions based on linear stability theory agreed with the observed trend of decreasing drop size with increasing jet velocity and impingement angle. However, the model overpredicted the measured drop sizes.

---

[*] Graduate Student, Mechanical Engineering, Student Member AIAA

[**] Research Associate, Mechanical Engineering, Member AIAA

[†] Professor, Mechanical Engineering, Member AIAA

Nomenclature

English Symbols

d	diameter
F	thickness distribution
h	sheet thickness
k	wavenumber
l	length
L	length of injection element
r	radial distance from impingement point
Re	Reynolds number ($=U_j d_o/\nu_l$) based on liquid properties, jet velocity, and orifice diameter
Re_s	Reynolds number ($=U_s h/\nu_l$) based on liquid properties, sheet velocity, and sheet thickness
s	ratio of gas density to liquid density
t	time
U	velocity
W	maximum width of sheet
We	Weber number ($=\rho_l U_j^2 d_o/\sigma$) based on liquid properties, jet velocity and orifice diameter
We_s	Weber number ($=\rho_l U_s^2 h/\sigma$) based on liquid properties, sheet velocity and sheet thickness
x	axial distance from impingement point
y	coordinate perpendicular to x in the plane of the sheet

Greek Symbols

α	fan inclination angle
β	complex growth rate factor ($\beta=\beta_r+i\beta_i$)
η	disturbance amplitude
λ	wavelength
μ	dynamic viscosity
ν	kinematic viscosity
ϕ	angular coordinate on sheet
ψ	angle between wave front and radial vector from impingement point
ρ	density
θ	impingement half-angle
σ	surface tension

combustion instability phenomena associated with this type of injector. In addition, the degree to which current modeling approaches represent the breakup and drop formation processes occurring in these sprays is evaluated. To aid in the comparison of current work with previous studies, a review of previous experimental and theoretical work on liquid sheet breakup is presented next. The theoretical section brings together the results of several workers and provides the expressions later used to develop comparative theoretical predictions of liquid sheet shape, breakup length and drop size formation, while the experimental section summarizes the results and observations of previous workers.

Theoretical Models of Liquid Sheet Breakup

The physics behind the breakup of liquid sheets formed by the impingement of two high Weber number liquid jets is not well understood. Related theoretical treatments of liquid sheet atomization include Childs and Mansour's[10] numerical simulation, and a Kelvin-Helmholtz instability analysis using a vortex discretization technique by Rangel and Sirignano.[11] However, linear stability theory based on the growth of infinitesimal disturbances due to aerodynamic stresses on the liquid sheet surface is most commonly used.[12-15] The disturbance on the sheet surface, η, is given by

$$\frac{\eta}{\eta_o} = e^{\beta_i t} \tag{1}$$

where η_o is the initial displacement amplitude, β_i is the growth rate and t is time.

Typically the growth rate, β_i, is calculated for a spectrum of wavenumbers, k. The disturbance wavenumber, k_m, with the maximum growth rate, $\beta_{i,m}$, controls the breakup process. Both sinuous (antisymmetric) and dilatational (symmetric) waves can grow; however, previous researchers have shown that sinuous waves grow faster than dilatational waves,[12] hence only the behavior of sinuous disturbances are considered hereafter. The theory does not predict a critical disturbance amplitude for sheet disintegration, and consequently, an empirical relation of the following form is used:[13]

$$\int_0^{t_b} \beta_{i,m} dt = 12 \tag{2}$$

where t_b is the sheet breakup time. The above relation can also be recast in terms of a spatial distance

$$\int_0^{x_b} \frac{\beta_{i,m}}{U_s} dx = 12 \tag{3}$$

where x_b is the breakup distance and U_s is the sheet velocity. Thus, through the above empirical equation, the length of the intact sheet can be determined once a relation for the maximum growth rate, $\beta_{i,m}$, is ascertained. The wavenumber, k_m, associated with the fastest growing disturbance is used to subsequently predict the size of ligaments and drops shedding from the edge of the intact sheet.[13]

The derivation of an expression for the growth rate factor and the wavenumber has been done for an inviscid constant thickness sheet,[12] and an attenuating viscous sheet.[13,14] Other researchers have extended these equations describing sheet breakup to the case of the sheets formed by impinging jets.[8,9] A concise summary of the appropriate equations and their underlying assumptions is given next.

Squire[12] investigated the instability of constant thickness, inviscid liquid films due to growth of antisymmetric disturbances. He derived expressions for the wavenumber and corresponding growth rate coefficient for the most unstable wave. The wavenumber, k_m, for the most unstable wave was given as

$$k_m = \frac{\rho_g U_s^2}{2\sigma} \tag{4}$$

where ρ_g is the gas density and σ is the surface tension. The corresponding maximum growth rate factor was given by

$$\beta_{i,m} = \frac{\rho_g U_s^2}{\sqrt{2\rho_l \sigma h}} \tag{5}$$

where ρ_l is the liquid density and h is the sheet thickness. The above two relations are valid for $We_s = \rho_l U_s^2 h/\sigma > 1$, and for disturbance wavelengths large compared to the sheet thickness. Squire[12] compared his predictions of the wavelength of the most unstable disturbance, λ_m ($=2\pi/k_m$), to those measured from photographs of liquid sheets produced by a nozzle, and showed, in general, good agreement.

Taylor[7] studied jets colliding at impingement angles of 60°, 90° and 120°, at jet velocities up to 5.6 m/s. He made detailed measurements of sheet shape, including its thickness and lateral spread, and compared these measurements to values predicted on the basis of unity Weber number, We_s, at the edge of the sheet.[7] His measurements showed that the sheet thickness, h, at any radial location, r, on the sheet was of the form, $rh = F(\theta,\phi)$, which is independent of

$$d_L = \sqrt{\frac{4h}{k}} \qquad (9)$$

Larger ligaments are produced for increasing sheet thickness and decreasing wavenumber. The ligaments subsequently break up into drops as a result of surface tension induced symmetrical wave growth. Dombrowski and Johns[13] assumed that the wave grows until the disturbance amplitude is equal to the ligament radius, thus resulting in one drop per wavelength. The drop size, d_D, for water in air is then

$$d_D = \left(\frac{3\pi}{\sqrt{2}}\right)^{\frac{1}{3}} d_L \left[1 + \frac{3\nu_l \rho_l}{\sqrt{\rho_l \sigma d_L}}\right]^{\frac{1}{6}} = 1.89 d_L \qquad (10)$$

where d_L is the ligament diameter from Eq. 9.

Ibrahim and Przekwas[9] analytically treated the disintegration of liquid sheets formed by two impinging jets. In terms of the Weber number, We, based on the orifice diameter, jet velocity and liquid properties, they suggested the presence of two breakup regimes. Their suggestion was based on Huang's[6] experiments on opposed jets, that showed that the breakup mechanism for $We < 500$ was different than that for $We > 2000$. For a low Weber number regime ($We < 2000$), the authors[9] extended the work by Taylor[17] to obtain an analytical solution for the shape of the sheet, while for the high Weber number regime ($We > 2000$), they suggested the use of Weihs' analysis.[14] In the low Weber number regime, the authors suggested that stationary antisymmetric waves determine the shape of the sheet. Both Taylor[17] and Huang[6] also stated the importance of stationary antisymmetric waves in the low Weber number regime. Huang[6] observed that these waves, which take the form of cardioid waves for the directly opposed jet case, predominate between Weber numbers of 500 to 800.

In developing an expression for the sheet shape formed by two impinging jets, Ibrahim and Przekwas[9] first extended Naber and Reitz's[19] expression for an initial sheet thickness to the case of an impinging jet geometry. The initial sheet thickness, h_o, is related to angular position, ϕ, by

$$h_o = \frac{(\gamma(\frac{d}{2})\sin\theta)e^{\gamma(1-\frac{\phi}{\pi})}}{e^{\gamma}-1} \qquad (11)$$

where d_j is the diameter of the jet, θ is the impingement half-angle, and γ is a decay factor. Ibrahim and Przekwas[9] determined γ from mass and

momentum conservation equations to be uniquely related to the impingement half-angle, θ, as

$$\cos\theta = \left(\frac{e^{\gamma}+1}{e^{\gamma}-1}\right)\left(\frac{1}{1+(\frac{\pi}{\gamma})^2}\right) \qquad (12)$$

They also gave a general expression for the sheet thickness as follows:[9]

$$\frac{h}{h_o} = \left(\frac{d_j}{2\sin\theta}\right)\frac{1}{r} \qquad (13)$$

where r is the radial coordinate originating at the impact point. Inspection of Eq. 13 indicates that the sheet thickness is inversely proportional to the distance from the impingement point. The calculated sheet thickness from Eq. 13 compares well with the sheet thickness measurements made by Taylor[7] and Miller.[20]

Hasson and Peck[21] also developed an expression for the sheet thickness distribution

$$h = \frac{d_j^2 \sin^3\theta}{4r(1-\cos\phi\cos\theta)^2} \qquad (14)$$

which shows the same $1/r$ dependence as the Ibrahim and Przekwas equation (Eq. 13). Equations 11-13 and 14 predict a similar sheet thickness along the spray centerline ($\phi = 0°$), as shown in Fig. 2.

Rewriting Eq. 13 as

$$r_b = \frac{d_j h_o}{2h_e \sin\theta} \qquad (15)$$

where h_e is the thickness at the edge of the sheet and r_b is the distance from the impingement point to the sheet edge, the shape of the entire sheet can be found by calculating r_b, once h_e is known.

To find the edge sheet thickness, h_e, Ibrahim and Przekwas[9] used an expression developed by Taylor[7] which describes the form of antisymmetric waves that remain at rest

$$h_e = \frac{2\sigma}{\rho_l U_j^2 \sin^2\psi} \qquad (16)$$

where ψ is the angle between the wave front and the radius vector, r, and h_e is the edge sheet thickness. The above equation is the same as Eq. 6, but recast in a different form. The authors[9] argued that ψ is dependent only on θ and ϕ, as

$$\psi = (\frac{\pi}{2})e^{\ln(\frac{2\theta}{\pi})(1-\frac{\phi}{\pi})} \qquad (17)$$

5

photographs of the different spray sheets, Dombrowski and Hooper[5] measured the sheet speed using high speed cinematography, and drop size as a function of jet velocity and impingement angle. Distinct sheet structure differences were seen between the laminar and turbulent impinging jet cases. The sheet formed from laminar impinging jets tended to produce much larger and smoother sheets as compared to the sheets formed by turbulent impinging jets. Measured sheet velocities tended to be between the velocity of the jet and the value of $U_j\cos\theta$.

Dombrowski and Hooper[5] suggested that sheet breakup does not scale with Reynolds number, but is dependent on the jet velocity profile and impingement angle. Note, however, that the only parameter changed in the Reynolds number was the velocity. For turbulent jets, waves formed at the impingement point, termed "impact waves" caused the sheet to disintegrate. However, for the laminar impinging jets, both "impact waves" and aerodynamic waves affected the sheet disintegration process. The authors[5] also stated that the wavelength of both "impact waves" and aerodynamic waves and the breakup length decrease with increasing jet velocity. However, breakup length measurements made from their photographs dispute the latter statement.

Huang[6] experimentally and analytically studied the breakup of liquid sheets formed by two opposing water jets ($2\theta = 180°$). In his study, water was fed through standard ASME sharp edged orifices ranging in diameter from 1.59 to 4.76 mm (0.063 in. to 0.1875 in.) at typical jet velocities between 2 to 20 m/s. Huang[6] presented the measured nondimensional breakup radius ($r_b/0.5d_o$) versus Weber number ($\rho_l U_j^2 d_o/\sigma$).

Huang's[6] results indicated two Weber number dependent breakup regimes connected by a transition regime. In the first regime, $100 < We < 500$, the circular sheets were stable with a nearly perfect circular edge. Here, the nondimensionalized breakup radius increased with increasing Weber number. Huang[6] occasionally saw disturbances originating from the impingement point in this regime. These disturbances are akin to the impact waves observed by Dombrowski and Hooper.[5] Huang[6] performed a force balance between the inertia and surface tension forces acting on the circular sheet to obtain an expression that related the nondimensional breakup radius to the Weber number (for $We < 900$)

$$\frac{r_b}{\frac{1}{2}d_o} = 0.167 We \qquad (18)$$

The transition regime spanned a Weber number range from 500 to 2000. Huang[6] noted that cardioid waves emerged and predominated in part of this region ($500 < We < 800$). The nondimensional breakup radius reached a maximum between Weber numbers of 800 and 1000. The transition regime is also the one in which antisymmetric waves first appeared.

Huang[6] referred to the second breakup regime, $We > 2000$ (the maximum We for his experiments was 30000), as the unstable liquid sheet regime where "the sheet flaps with a flag-like motion." In this regime, the nondimensional breakup radius decreased with increasing Weber number. A semi-empirical relation based on linear stability theory for the breakup radius was developed

$$\frac{r_b}{\frac{1}{2}d_o} = 14.2\, s^{-\frac{2}{3}} We^{-\frac{1}{3}} \qquad (19)$$

where s is the ratio of the gas density to the liquid density.

Taylor[7] performed experiments on laminar impinging water jets with jet velocities to 5.6 m/s. He measured the sheet thickness, the lateral spread, and the breakup radii (r_b) of stable sheets formed by jets impinging at included angles of 30°, 60°, and 90°. The sheet shape was determined by stationary antisymmetric waves. The sheets produced in these experiments had closed, pointed tips similar to the closed rim and periodic drop regimes observed by Heidmann et al.[4] Hasson and Peck[21] used Taylor's[7] data to verify their expression for the sheet thickness (see Eq. 14).

Anderson et al.[8] investigated the spray characteristics of turbulent impinging jets by measuring the sheet breakup length, X_b, maximum spray width, W, and drop size as a function of flow velocity and injector geometry (2θ, d_o, L/d_o and l_j). An analytical model based on linear stability theory was used to predict breakup length and drop size. The experimental apparatus and the operating conditions of the impinging jet system were very similar to those of Heidmann et al.[4] In this study, the authors[8] found the breakup length to increase with decreasing impingement angle and increasing jet velocity, up to the maximum velocity tested (18.5

been reviewed thoroughly in the literature,[24,25] hence only a few system details are mentioned here. The collection optics were oriented 30° off axis from the forward propagation direction of the laser beam, which is the optimum angle for measuring transparent drops.[24] The optical configuration of the transmitting and collection optics chosen allowed the measurement drop size range to span 40 to 1400 μm.

Drop size/velocity measurements for a set of parametric conditions were made in a previous study[8] at two locations downstream of the impingement point, $x = 16$ and 41 mm. At each downstream location, measurements were made at 6.4 mm increments in the plane of the sheet normal to the sheet centerline.[8] In this study, only the drop size measurements at a single spatial location ($x = 16mm$, along the sheet centerline) are presented as a function of jet velocity and impingement angle. At each measurement location, 8000 drops were measured, since at least 5500 data points are needed for $\pm 5\%$ accuracy in mean diameter measurements.[26]

Laminar Impinging Jets

A series of experiments involving laminar impinging jets was also undertaken using the experimental setup shown in Fig. 3. For these tests, 0.51 mm diameter precision bore glass tubes with an L/d_o ratio of 375 were used. This large L/d_o ratio ensures fully developed flow. These tubes are very similar to those used by Dombrowski and Hooper.[5] Each glass tube was attached to a 12.7 mm O.D., 10.4 mm I.D. brass tube with fittings. To ensure laminar flow through the precision bore glass tubes, an inlet glass tube was contoured such that the fluid transitioned smoothly from the brass tube to the glass tube. The transition angle between the inlet glass tube wall and the tube centerline was 17°. This contoured inlet tube was fused to the 0.51 mm I.D. precision bore glass tube.

Contouring the inlet extended the Reynolds number range for laminar flow up to 10000 as indicated by pressure drop measurements taken across the glass tube, and the glass-like appearance of the jets. Recall that $Re = 2300$ is the usual laminar/turbulent transition value. Often, a "bursting phenomenon" was observed when studying the appearance of the laminar jets, where the smooth laminar jet would suddenly and violently turn chaotic and turbulent at some distance from the tube exit.

This phenomenon has been documented in the literature, and is attributed to velocity profile relaxation effects.[26]

As with the turbulent impinging jets, instantaneous images of the laminar impinging jet spray were taken using the CID camera and strobe light. Approximately 17 images at each operating and geometric condition were acquired from which both the breakup length and maximum spray width were measured. An average value and standard deviation of the two measured quantities were determined, and compared to model predictions and previous experimental studies.

Results and Discussion

The disintegration of sheets formed by two impinging liquid jets is modeled using two existing models; a stationary antisymmetric wave-based theory for low Weber numbers,[9] and a linear stability-based theory for high Weber numbers.[8] The stationary antisymmetric wave-based theory yielded the shape of the sheet from which the breakup length and maximum spray width were obtained, while the linear stability-based theory yielded breakup length and drop size predictions. The breakup length predictions of both theories, and the drop size predictions from the linear stability-based model are compared to experimental measurements. Breakup length measurements were made for both laminar and turbulent impinging jets, while drop size measurements were made only for the turbulent impinging jet case. Finally, measurements of the distance between apparent wave-like structures on the sheet surface are presented for the turbulent impinging jet case as a function of jet velocity and orifice diameter.

General Spray Characteristics

The sheets typically produced by turbulent impinging water jets are shown in Fig. 4. Here, the orifice diameter is 0.64 mm and the jet velocities are 6.4 and 18.5 m/s. The free jet length prior to impingement, or pre-impingement length, l_j, is 25 mm, L/d_o is 80 and the impingement angle, 2θ, is 60°. The two instantaneous images shown in Fig. 4 fall into the *fully developed* regime identified by Heidmann et al.[4] It is interesting to note the apparent periodic nature of the disturbances on the sheet surface and the detaching ligaments. Recall that Heidmann et al.[4] measured the "wave

For the viscous sheets, the wavenumber of the most unstable wave, k_m, can be found from Eq. 8, which is taken from Weihs' analysis[14] and is identical to the results obtained by Dombrowski and Johns,[13] by differentiating β_i with respect to k and setting the result equal to zero, and subsequently solving for k_m. The maximum growth rate factor, $\beta_{i,m}$, can subsequently be found by substituting k_m back into Eq. 8.

The wavenumber and growth rate factor for the fastest growing wave for both viscous and inviscid cases were calculated and compared as a function of sheet velocity and sheet thickness for a water sheet in air. The behavior of the wavenumber for the fastest growing wave for the viscous case nondimensionalized by the same wavenumber for the inviscid case is shown in Fig. 6 as a function of U_s and h. The deviation between the wavenumber predictions of the viscous and inviscid models increases with increasing sheet thickness and velocity. For example, there is a 7% difference between the wavenumber predictions for the viscous and inviscid case for a sheet which is 2 mm thick traveling with a speed of 50 m/s. Thus, for thin, low speed sheets, Squire's[12] simple expression for the wavenumber (Eq. 4) of the most unstable wave is accurate. In fact, for all the cases in this study, the use of Squire's expression[12] results in less than 1% deviation.

The growth rate factor for the most unstable wave, $\beta_{i,m}$, is presented in Fig. 7 for both the viscous and inviscid cases as a function of sheet velocity and sheet thickness for water in air. For both the inviscid and viscous analyses, the most significant conclusion to draw from Fig. 7 is that the maximum growth rate factor, $\beta_{i,m}$, predicted by Squire's inviscid analysis,[12] and that predicted by Weih's[14] or Dombrowski and John's[13] viscous analysis, are the same for the conditions of this study. For the cases studied here, Squire's simple expressions for the wavenumber (Eq. 4) and growth rate factor (Eq. 5) of the most unstable wave will be used to calculate breakup length and drop size. The wave growth factor increases with increasing sheet velocity and decreasing sheet thickness. Slow moving sheets and/or thick sheets tend to retard wave growth. Although not evident in Fig. 7, viscosity also has a damping effect on wave growth at higher sheet velocities. However, for more viscous liquids and higher gas densities (corresponding to higher chamber pressures), the two analyses will differ.

The sheet breakup length is linked to the sheet velocity, disturbance growth rate, sheet thinning rate and the ratio of the final to the initial disturbance amplitude. Recall that the breakup length is defined as the distance from the impingement point to where the intact sheet disintegrates along the spray centerline. The empirical relation given by Eq. 3 is used to compute the breakup length, x_b, using the maximum growth rate factor, $\beta_{i,m}$ (see Eq. 5), derived by Squire.[12] Inspection of Eq. 5 indicates the need for a sheet thickness expression, since the fluid and medium parameters are known. For the sheet thickness, Hasson and Peck's[21] expression (Eq. 14) was used. With the three aforementioned equations, an explicit expression for the breakup length, x_b, is derived as follows:

$$\frac{x_b}{d_o} = 5.451 s^{-\frac{2}{3}} [We\, f(\theta)]^{-\frac{1}{3}} \quad (20)$$

where d_o is the orifice diameter, s is the ratio of gas density to liquid density, We is the Weber number based on liquid properties, jet velocity and orifice diameter, and $f(\theta)$ is given as follows:

$$f(\theta) = \frac{(1-\cos\theta)^2}{\sin^3\theta} \quad (21)$$

where θ is the impingement half-angle. Note that the constant given by Eq. 21 is contained in the sheet thickness equation of Hasson and Peck[21] (Eq. 14) for $\phi = 0°$ (spray centerline). If a different expression for the sheet thickness was used, then $f(\theta)$ would have a different form. For conditions involving more viscous liquids and/or higher gas densities, the expression for the growth rate factor, β_i, for the viscous case given by Eq. 8, and Hasson and Peck's[21] sheet thickness relation (Eq. 14) can also be used in conjunction with the empirical breakup relation, Eq. 3. The resulting expression is then numerically integrated as a function of wavenumber to solve for the breakup length.[8]

Sheet Breakup Length Measurements

Sheet breakup length was calculated using Eq. 20, and compared to breakup length measurements made for both laminar and turbulent impinging jets. The numerical integration procedure outlined for the viscous case was also carried out and, as expected, the breakup length was identical to that predicted by Eq. 20. The nondimensional breakup length, x_b/d_o, is plotted as a function of the nondimensional scaling parameter $We(1-\cos\theta)^2/\sin^3\theta$ in Fig. 8. For the experimental measurements, each symbol represents an average of 17 measurements, and the

case, the measured non-dimensional breakup lengths for various jet diameters lie on nearly a single curve for this fixed impingement angle. The same trend is observed at the other impingement angles although different curves were observed for each angle. It should be noted that this collapse of the turbulent impinging jet results to a single curve for a fixed impingement angle is a reflection of the We number dependence since the geometric factor in the nondimensional scaling factor remains constant for fixed impingement angle. The orifice diameter was not varied in the laminar case, so only one curve is shown in Fig. 9. Similar to Huang's[6] breakup radius results for opposed jets, and the present results for laminar impinging jets, it is likely that the breakup length for the turbulent impinging jet case will peak for some Weber number and then decrease.

Maximum spray width measurements, W, were made for the laminar and turbulent impinging jet cases as shown in Fig. 10. The maximum spray widths of the sheets formed by the laminar impinging jets were typically much larger than their turbulent counterparts. For the turbulent case, the maximum spray width was relatively independent of changes to jet velocity and impingement angle, and increased slightly with increasing orifice diameter (not shown in Fig. 10). In the laminar impinging jet case, the maximum spray width increased with increasing jet velocity and impingement angle. For the range of conditions studied, W does not reach a maximum value, in contrast to the observations for the breakup length for the laminar case. The results shown in Fig. 10 indicate that the "impact waves" do not have as significant an effect on the sheet width as the sheet length.

Ibrahim and Przekwas[9] proposed that their extension of Taylor's[18] stationary antisymmetric wave-based theory should be used in a low Weber number regime ($We < 2000$), while linear stability theory should be applied to a high Weber number regime. In the low Weber number regime ($We < 2000$), the shape of the sheet is predicted using Eqs. 11, 12 and 15-17. The sheet shape predicted using the aforementioned equations is shown in Fig. 11 as a function of the impingement angle for an orifice diameter of 0.51 mm and a jet velocity of 7.1 m/s. Note that the impingement point is at $x = 0$, $y = 0$. The predicted sheet shape for $2\theta = 60°$ looks similar to the corresponding image for the same conditions shown in Fig. 5 (low jet velocity case, $U_j = 7.1$ m/s). From the shape of the sheet, both the breakup length, x_b, and maximum sheet width, W,

can be obtained. The predicted sheet shapes have pointed tips, except for the opposed jet case ($2\theta = 180°$). For the laminar impinging jet case (experimental), sheets with pointed tips were observed for all impingement angles tested up to a Weber number of about 350. For Weber numbers greater than 350, the sheets disintegrated before a pointed tip was formed.

Further perusal of Fig. 11 indicates that the breakup length increases with increasing impingement angle up to about 100°, after which it decreases. However, the maximum sheet width increases with increasing impingement angle up to a maximum at $2\theta = 180°$ (opposed impinging jets). For the impingement angles studied in the present experiments ($2\theta = 40°$, 60°, 80° and 100°) for the laminar impinging jet case, the general trend was for increasing breakup length with increasing impingement angle, the same trend predicted by the model. Since breakup length measurements were not made for impingement angles greater than 100°, the decrease in breakup length with increasing impingement angle for impingement angles greater than 100° as predicted by the model cannot be either confirmed or contradicted.

A comparison between the breakup length predicted by linear stability-based theory, Ibrahim and Przekwas'[9] extension of Taylor's[18] stationary antisymmetric wave theory, and the breakup length measurements for the laminar and turbulent cases is shown in Fig. 12. Specifically, the nondimensional breakup length, x_b/d_o, is plotted as a function of Weber number for an impingement angle of 60°. Recall that Ibrahim and Przekwas[9] stated that a Weber number of 2000 may be an appropriate dividing line for the employment of either the stationary antisymmetric wave-based model or the linear stability-based theory. Note that the breakup length predictions from the two models intersect at a Weber number of approximately 500 for the case shown.

As seen in Fig. 12, the breakup length as predicted by the Ibrahim and Przekwas model[9] is linearly proportional to Weber number, whereas for the linear stability-based model, it is proportional to $We^{-1/3}$. The breakup length predictions from the Ibrahim and Przekwas[9] model overpredict the breakup length measurements made for both the laminar and turbulent cases; however, the measured breakup length does increase with increasing Weber number, but not as strongly as the stationary

13

The surface wave category included disturbances on the intact sheet surface. Typically, the distance between adjacent surface waves, λ_{sw}, increased with increasing distance from the impingement point. Separation distance measurements were made over the entire intact sheet whenever possible to obtain an average λ_{sw}. The separation distance of adjacent surface waves is plotted as a function of jet velocity and orifice diameter for an impingement angle of 60° in Fig. 15. Each point plotted represents an average between 10 and 50 separate measurements, depending on operating conditions, while the corresponding bars represent the ± standard deviation. Despite the large standard deviation, there appears to be a distinct increase in λ_{sw} with increasing orifice diameter. However, for the cases studied, the separation distance is relatively insensitive to changes in jet velocity. Although not presented in graphical format, it was also found that the separation distance, λ_{sw}, was insensitive to changes in impingement angle.

Similar measurements were made for the edge and detached ligament categories. Edge ligaments were defined as strands of liquid attached to the intact sheet periphery. Detached ligaments were strands of fluid either completely or nearly completely separated from the downstream edge of the intact sheet. In general, the average separation distance between adjacent detached ligaments was larger than that of the edge ligaments. Likewise, the average separation distance between adjacent edge ligaments was larger than that of the surface waves. Again, the trends observed for λ_{sw} were also observed for the edge ligament category, i.e., separation distance increased with increasing orifice diameter, but was insensitive to changes in jet velocity and impingement angle. The behavior of the separation distance between adjacent detached ligaments was not as apparent as the other two categories since not enough measurements were made to yield a meaningful average and standard deviation. It is interesting to note that the measured separation distances of the surface waves and edge ligaments are similar in magnitude to the fastest growing wavelength predicted by Squire[12]

$$\lambda_m = \frac{4\pi\sigma}{\rho_g U_j^2} \qquad (25)$$

However, the wavelength of the most unstable wave predicted by Eq. 25 is strongly dependent on sheet velocity and independent of the orifice diameter. This is contrary to the observed behavior of the various measured separation distances.
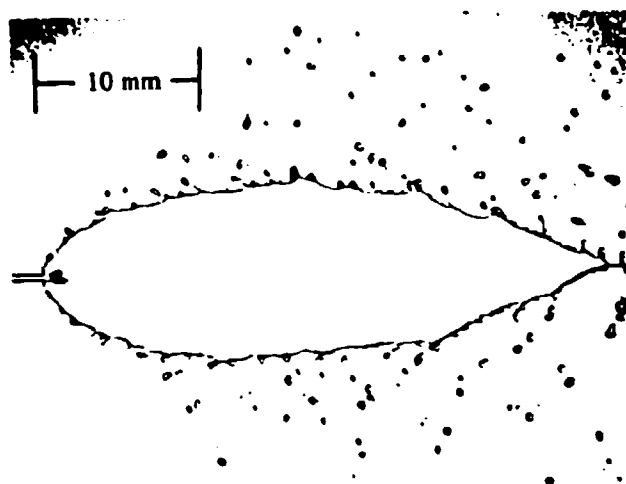
Summary and Conclusions

A systematic study of the atomization of impinging liquid jets investigating the effects of jet conditions (laminar versus turbulent), orifice diameter, impingement angle and jet velocity has been conducted. Results of the present study have been compared to current theories in terms of sheet breakup length, drop size and sheet shape. Experiments contrasting laminar and turbulent jet conditions clearly demonstrate that the jet conditions have a dramatic effect on the atomization process. The present results are in complete agreement with earlier studies by Dombrowski and Hooper[5] with regards to the effects of jet conditions on impinging jet atomization. These results encourage speculation that velocity profile and turbulence intensity characteristics of the jets strongly affect the atomization processes for impinging jet injectors. However, quantitative assessment of the specific mechanisms controlling atomization remain to be established.
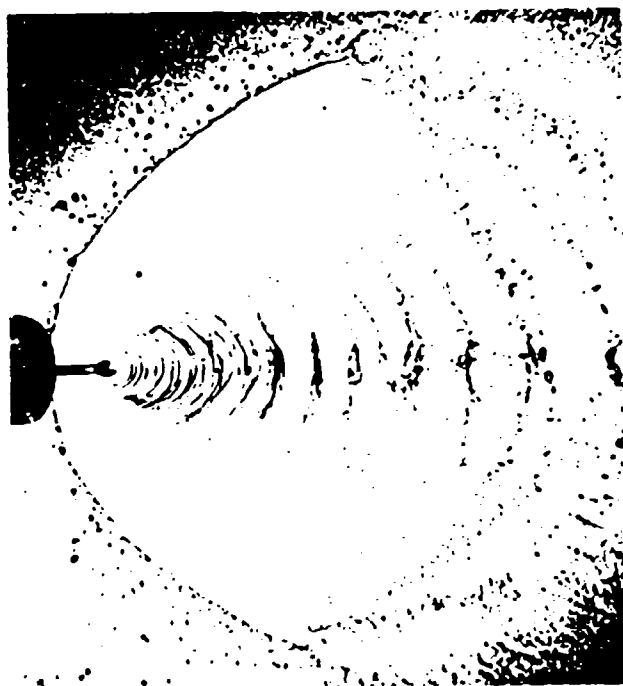
Measurements of the breakup length and spray width also showed distinct differences for laminar and turbulent jet conditions. The breakup length for laminar impinging jet conditions initially increased with increasing Weber number (i.e., jet velocity) achieving a maximum for Weber numbers between 550 and 725. For larger Weber numbers, the breakup length was observed to decrease. while for the full Weber number range tested, the breakup length increased with increasing impingement angle. The maximum width of the sheet for the laminar impinging jet case increased with increasing impingement angle and jet velocity. For the turbulent impinging jet case, the breakup length continually increased with increasing Weber number ($350 < W_e < 6700$) while decreasing with increasing impingement angle, whereas, the maximum width of the sheet was relatively constant for a fixed orifice diameter.

For low Weber number ($We < 350$) laminar impinging jet conditions, predictions based on stationary antisymmetric wave-based theory compared reasonably well in terms of the observed sheet shape, sheet breakup length, and breakup length and maximum sheet width behavior as a function of impingement angle. For Weber numbers greater than 350, agreement between the laminar impinging jet case with the stationary antisymmetric wave-based theory was significantly less satisfactory.

15

3. Liquid Propellant Rocket Instability, D. T. Harrje and F. H. Reardon (eds.), NASA SP-194, 1972.

4. Heidmann, M. F., Priem, R. J. and Humphrey, J. C., "A Study of Sprays Formed by Two Impinging Jets," NACA Technical Note 3835, March 1957.

5. Dombrowski, N. and Hooper, P. C., "A Study of the Sprays Formed by Impinging Jets in Laminar and Turbulent Flow," J. Fluid Mechanics, Vol. 18, Part 3, 1963, pp. 392-400.

6. Huang, J. C. P., "The Breakup of Axisymmetric Liquid Sheets," J. Fluid Mechanics, Vol. 43, Part 2, 1970, pp. 305-319.

7. Taylor, G. I., "Formation of Thin Flat Sheets of Water," Proc. Roy. Soc. A, 259, 1960, pp. 1-17.

8. Anderson, W. E., Ryan, H. M., Pal, S. and Santoro, R. J., "Fundamental Studies of Impinging Liquid Jets," AIAA paper 92-0458, 30th Aerospace Sciences Meeting, Reno, NV, Jan. 6-9, 1992.

9. Ibrahim, E. A. and Przekwas, A. J., "Impinging Jets Atomization," Phys. Fluids A, Vol. 3, No. 12, Dec. 1991.

10. Childs, R. E. and Mansour, N. N., "Simulation of Fundamental Atomization Mechanisms in Fuel Sprays," J. Propulsion, Vol. 5, No. 6, Nov.-Dec. 1989, pp. 641-649.

11. Rangel, R. H. and Sirignano, W. A., "Nonlinear Growth of Kelvin-Helmholz Instability: Effect of Surface Tension and Density Ratio," Phys. Fluids, Vol. 31, No. 7, 1988, pp. 1845-1855.

12. Squire, H. B., "Investigation of the Instability of a Moving Liquid Film," British J. of Applied Physics, Vol. 4, 1953, pp. 167-169.

13. Dombrowski, N. and Johns, W. R., "The Aerodynamic Instability and Disintegration of Viscous Liquid Sheets," Chem. Eng. Science, Vol. 18, 1963, pp. 203-214.

14. Weihs, D., "Stability of Thin, Radially Moving Liquid Sheets," J. Fluid Mech., Vol. 87, Part 2, 1978, pp. 289-298.

15. Levich, V. G., Physicochemical Hydrodynamics, Prentice-Hall, Englewood Cliffs, NJ, 1962, Chapter 11.

16. Taylor, G. I., "The Dynamics of Thin Sheets of Fluid III. Disintegration of Fluid Sheets," Proc. Roy. Soc. A, 253, 1959, pp. 313-321.

17. Taylor, G. I., "The Dynamics of Thin Sheets of Fluid II. Waves on Fluid Sheets," Proc. Roy. Soc. A, 253, 1959, pp. 296-312.

18. Brodkey, R. S., Phenomena of Fluid Motions, Addison-Wesley Series in Chemical Engineering, 1967.

19. Naber, J. D. and Reitz, R. D., SAE paper 880107, 1988.

20. Miller Jr., K. D., J. Applied Phys., Vol. 31, p. 1132, 1960.

21. Hasson, D. and Peck, R. E., "Thickness Distribution in a Sheet Formed by Impinging Jets," AIChE Journal, September 1964, pp. 752-754.

22. Ferrenberg, A., Hunt, K. and Duesberg, J., "Atomization and Mixing Study," Contract NAS8-34504, 1985.

23. Nurick, W. H., "Orifice Cavitation and Its Effects on Spray Mixing," J. of Fluids Eng., December 1976, pp. 681-687.

24. Bachalo, W. D. and Houser, M. J., "Phase/Doppler Spray Analyzer for Simultaneous Measurement of Drop Size and Velocity Distributions," Optical Engineering, Vol. 23, 1984, pp. 583-590.

25. Ibrahim, K. M., Werthimer, G. D. and Bachalo, W. D., "Signal Processing Considerations for Laser Doppler and Phase Doppler Applications," The Fifth International Symposium on the Application of Laser Techniques of Fluid Mechanics, Lisbon, Portugal, July 9-12, 1990.

26. Lefebvre, A. H., Atomization and Sprays, Hemisphere Publishing Corporation, Philadelphia, PA, 1989.
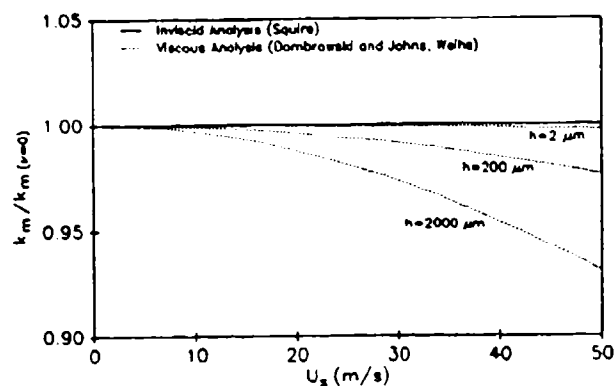
5a) $U_j = 7.1$ m/s

Fig. 6. The wavenumber of the fastest growing disturbance calculated for the viscous case, nondimensionalized with the wavenumber of the fastest growing disturbance for the inviscid case plotted as a function of sheet velocity, U_s, and sheet thickness, h. Note that the ordinate axis ranges from 0.90 to 1.05. Results are for a water sheet in air.
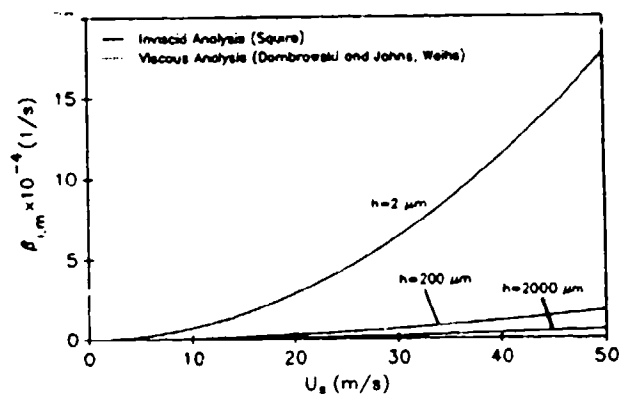

5b) $U_j = 17.9$ m/s

Fig. 5. Instantaneous images of sprays formed by two laminar impinging water jets. The jets emanated from 0.51 mm inner diameter, $L/d_o = 375$ precision bore glass tubes. The impingement angle, 2θ, was 60°, while the pre-impingement length, l_j, was approximately 10 mm. Note that the scale of these images is the same as those in Fig. 4. In addition, the orifice diameter and jet velocities are similar for the images in both Fig. 4 and this figure. Flow is from left to right.

Fig. 7. The maximum growth rate factor, $\beta_{i,m}$, plotted as a function of sheet velocity, U_s, and sheet thickness, h, for inviscid and viscous cases. Results for a water sheet in air.
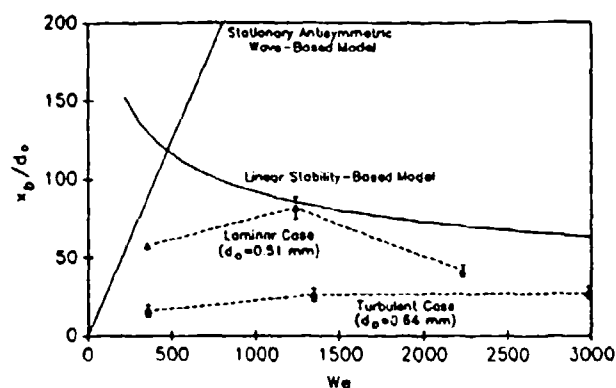
Fig. 12. The nondimensional breakup length as predicted by the linear stability-based model and the stationary antisymmetric wave-based model compared to measurements from both laminar and turbulent impinging jet cases plotted as a function of Weber number. The impingement angle is 60° for all results shown.
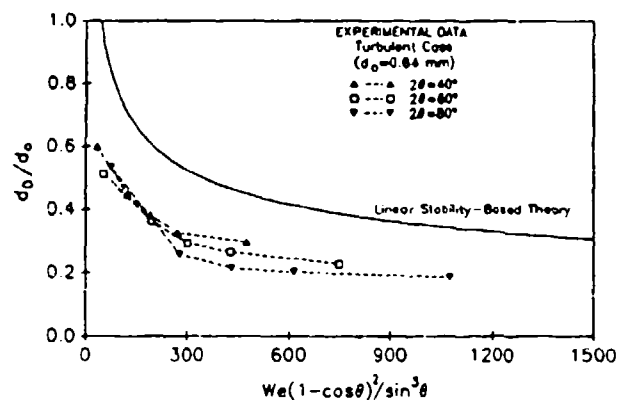

Fig. 14. A typical spray formed by two turbulent impinging water jets issuing from 0.64 mm diameter, $L/d_o = 80$ glass tubes. The impingement angle was 60° and the pre-impingement length was 25 mm. Flow is from left to right. The distance between adjacent surface waves, edge ligaments and detached ligaments were measured from such spray images.

Fig. 13. Nondimensional drop size, d_D/d_o, plotted as a function of a nondimensional scaling factor and impingement angle. Drop size predictions made using linear stability-based theory and drop size measurements made using the PDPA are shown.
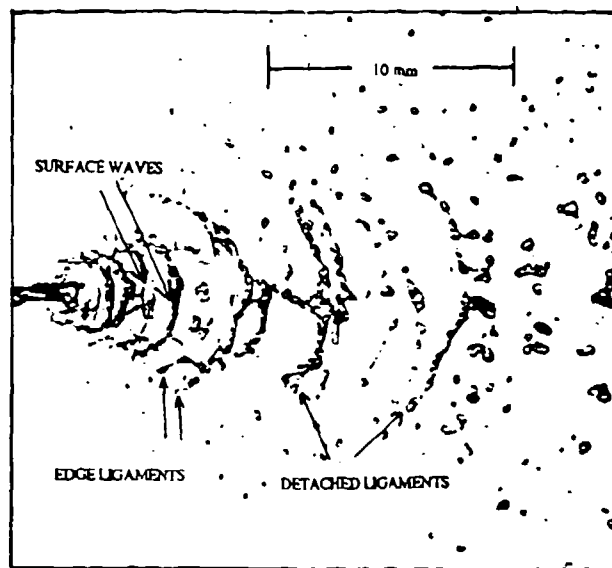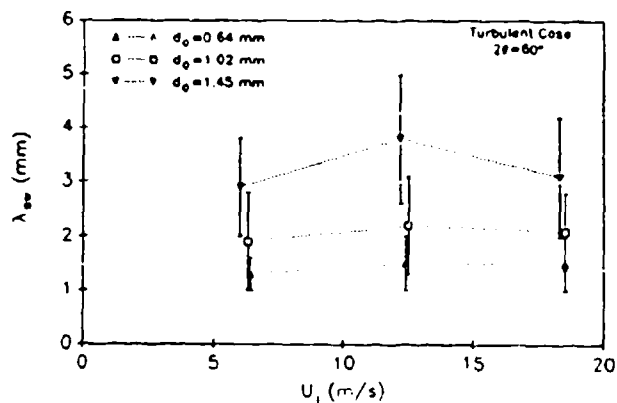

Fig. 15. The separation distance between adjacent surface waves, λ_{sw}, plotted as a function of jet velocity and orifice diameter for the turbulent impinging jet case at an impingement angle of 60°. Each point plotted represents an average between 10 to 50 separate measurements, while the corresponding bars indicate the associated standard deviation.

21

END

FILMED

DATE:

9-93

DTIC